Texture Classification and Retrieval Using Shearlets and Linear Regression

Yongsheng Dong, Dacheng Tao, *Senior Member, IEEE*, Xuelong Li, *Fellow, IEEE*, Jinwen Ma, and Jiexin Pu

***Abstract*—Statistical modeling of wavelet subbands has frequently been used for image recognition and retrieval. However, traditional wavelets are unsuitable for use with images containing distributed discontinuities, such as edges. Shearlets are a newly developed extension of wavelets that are better suited to image characterization. Here, we propose novel texture classification and retrieval methods that model adjacent shearlet subband dependences using linear regression. For texture classification, we use two energy features to represent each shearlet subband in order to overcome the limitation that subband coefficients are complex numbers. Linear regression is used to model the features of adjacent subbands; the regression residuals are then used to define the distance from a test texture to a texture class. Texture retrieval consists of two processes: the first is based on statistics in contourlet domains, while the second is performed using a pseudo-feedback mechanism based on linear regression modeling of shearlet subband dependences. Comprehensive validation experiments performed on five large texture datasets reveal that the proposed classification and retrieval methods outperform the current state-of-the-art.**

***Index Terms*—Contourlets, linear regression, shearlets, subband dependence, texture classification, texture retrieval.**

I. Introduction

TEXTURE represents spatial variations in pixel intensity and orientation and is used in a variety of image and video analysis applications [1], [2], including contour detection [3], image retrieval [5], [6], object recognition [7], [10], [12], image segmentation [14], image editing [11], pedestrian detection [8], gait recognition [9], scene classification [13], video texture categorization [16], and video indexing [15]. Texture is generally used to represent a subregion of an image, and as a consequence the image as a whole is considered a mosaic of different texture regions [5]. Texture is also extracted from an image as an important pixel feature channel [3], [4], and spacetime texture has been used for video indexing and retrieval [15], [17].

Texture classification and retrieval have therefore become integral to computer vision and image recognition applications, and are performed using a variety of methods, including structural [20], [21], statistical [19], model-based [18], [22], [23], and multiscale transform-based methods [24]–[36]. Multiscale transform-based methods have gained particular popularity, since the multiresolution and orientated representations of the transforms are consistent with the human perception of images. The most commonly used multiscale transforms include the Gabor transform [24], the wavelet transform [25]–[34], the ridgelet transform [35], and the contourlet transform [36].

When multiscale transform-based methods are used for texture classification and retrieval, statistical models are usually used to model subband coefficients in the transformed domains. The models usually used in the wavelet domains include the generalized Gaussian density model [30], the bit-plane probability (BP-P) model [31], the refined histogram [34], and the generalized gamma density model [40]. The models used in the contourlet domains include the hidden Markov model [36] and the Poisson mixture model [41]. In addition, energy feature-based methods are also used for texture classification and retrieval [25], [27].

Since the contourlet transform can capture the geometrical smoothness of the contours and has a better approximation rate than the wavelet transform [37], [38], it has gained traction in image processing and recognition, including for image denoising [36], handwritten numeral recognition [39], texture classification [40], [41], and texture retrieval [42]. However, when a contourlet transform is performed on an image, the size of the resulting contourlet subbands reduces with increasing decomposition scale. This can result in too few coefficients in each subband at the coarsest scale to be modeled easily, and they are statistically unstable for textures from the same texture class.

As a newly developed 2-D extension of the wavelet transform, the shearlet transform effectively captures the intrinsic

Manuscript received November 23, 2013; revised March 3, 2014 and May 15, 2014; accepted May 16, 2014. Date of publication July 11, 2014; date of current version February 12, 2015. This work was supported in part by the National Natural Science Foundation of China under Grant 61125106 and Grant 61301230, in part by China Post-Doctoral Science Foundation under Grant 2014M550517, in part by the Key Research Program of the Chinese Academy of Sciences under Grant KGZD-EW-T03, in part by the Key Science and Technology Research Project of Henan Province's Education Department of China under Grant 13B520992, and in part by the Research Fund for the Doctoral Program of Henan University of Science and Technology of China under Grant 09001673. This paper was recommended by Associate Editor Q. Zhao.

Y. Dong is with the Information Engineering College, Henan University of Science and Technology, Luoyang 471023, China, and also with the Center for OPTical IMagery Analysis and Learning, State Key Laboratory of Transient Optics and Photonics, Xi'an Institute of Optics and Precision Mechanics, Chinese Academy of Sciences, Xi'an 710119, China (e-mail: dongjunyu@ouc.edu.cn).

J. Pu is with the Information Engineering College, Henan University of Science and Technology, Luoyang 471023, China.

D. Tao and X. Li are with the Center for OPTical IMagery Analysis and Learning, State Key Laboratory of Transient Optics and Photonics, Xi'an Institute of Optics and Precision Mechanics, Chinese Academy of Sciences, Xi'an 710119, China (e-mail: xuelong_li@opt.ac.cn).

J. Ma is with the Department of Information Science, School of Mathematical Sciences and LMAM, Peking University, Beijing 100871, China.

Color versions of one or more of the figures in this paper are available online at http://ieeexplore.ieee.org.

Digital Object Identifier 10.1109/TCYB.2014.2326059

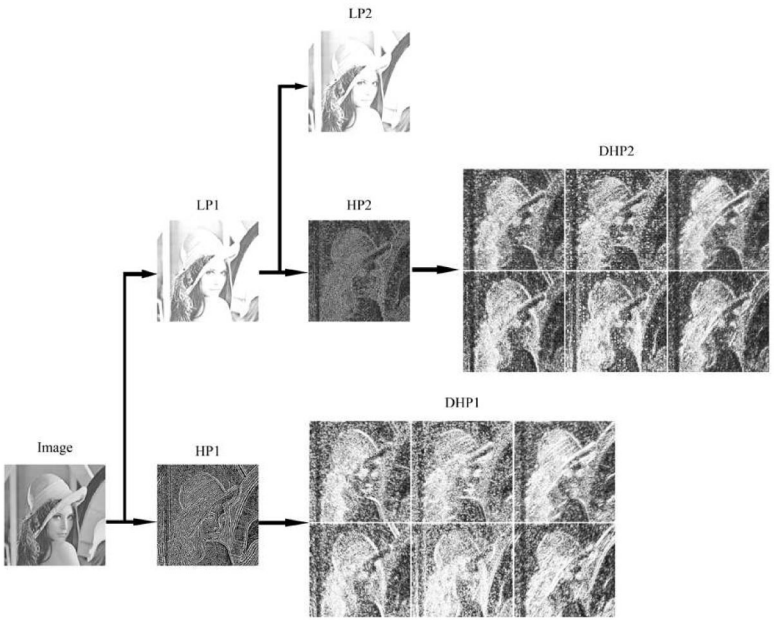

Fig. 1. Shearlet decomposition of the *Lena* image. HP1: high-pass subbands at the first scale. DHP1: directional high-pass subbands at the first scale. LP1: low-pass subband at the first scale. HP2: high-pass subbands at the second scale. DHP2: directional high-pass subbands at the second scale. LP2: low-pass subband at the second scale. Coefficients with small modulus are colored black while coefficients with large modulus are colored white.

geometric structure key to the interpretation and analysis of visual information. Moreover, the shearlet expansion can achieve the optimal approximation rate for piecewise smooth functions with C^2 contours [43], and the size of every shearlet subband is the same as the initial image, thereby overcoming a disadvantage of contourlets. However, the coefficients produced are complex numbers with complicated relationships, and are therefore inconvenient for computer vision and image recognition purposes. In order to overcome this limitation, here we study shearlet subbands and their dependence relationships using a statistical method.

We propose a novel texture classification and retrieval method by modeling the dependences of adjacent shearlet subbands using linear regression. In order to conveniently model these dependences, we represent each shearlet subband with two extracted energy features. Linear regression is then used to model the dependences of the energy features in adjacent subbands in the same direction, with the weighted regression residuals used to define the distance from a test texture to a texture class. Our proposed texture retrieval method consists of two successive retrieval processes. The first is implemented using our recently proposed statistical texture retrieval method in contourlet domains. The second is performed using a pseudo-feedback mechanism based on linear regression modeling of shearlet subband dependences.

We clearly demonstrate that our texture classification and retrieval approaches are superior to several current state-of-the-art methods by comprehensive experimental validation in five large texture datasets. In particular, four major contributions are made in this paper. First, we discover the linear dependences of adjacent subbands in the shearlet domain. Second, we propose a texture classification method based on shearlets and linear regression models. Third, we propose a pseudo-feedback mechanism to perform texture retrieval using linear regression modeling of shearlet subband dependences. Finally, we propose a preretrieval method for image texture based on statistics in the contourlet domain.

The remainder of the paper is organized as follows. Section II introduces the shearlet transform. In Section III, we present a new texture classification method based on linear regression modeling of shearlet subband dependences. Section IV presents our proposed texture retrieval method with a pseudo-feedback mechanism based on linear regression models. The experimental results presented in Section V demonstrate the effectiveness of our proposed texture classification and retrieval methods. Finally, we briefly conclude in Section VI.

II. Shearlet Transform

The shearlet transform was recently developed to overcome limitations inherent in wavelets. The shearlet representation is based on a simple but rigorous mathematical framework. This framework not only provides a more flexible theoretical tool for the geometrical representation of multidimensional data, but is also more natural for implementation. In one sense, the theory of shearlets can be seen as a theoretical justification for contourlets [43]. Moreover, the shearlet transform can be implemented using the succession of a Laplacian pyramid and directional filtering.

Fig. 1 shows an example of the use of the shearlet transform on the *Lena* image. For clarity, only two-scale decomposition is used with six directional subbands at each scale. Note that for each directional subband, we only show the modulus of subband coefficients due to directional subband coefficients being complex numbers. Small moduli are colored black, while large moduli are colored white. As can clearly be seen in Fig. 1, the size of each shearlet subband is the same as the initial image. Moreover, we notice that the shearlet decomposition produces coefficients with large moduli to represent the

contour and directional information of the image. It is therefore valuable to study how to represent the shearlet subbands and their relationships in a simple yet effective way.

More recent developments and applications of the shearlet transform can be found in [44]–[46]. In the next section, we will study the shearlet subbands and their relationship to linear regression modeling.

III. Texture Classification Based on Linear Regression Modeling the Dependence Between Shearlet Subbands

Although the relationships of shearlet coefficients are given in [43], the resulting coefficients are complex numbers and their relationships are complicated. This precludes the convenient use of the shearlet transform in image recognition. As an alternative, here we study their dependences from a statistical viewpoint, and apply it to texture classification and retrieval. We first consider how to represent each shearlet subband.

A. Energy Representations of Shearlet Subbands

The total energy of wavelet subbands is usually used to represent them for texture classification [27]–[29]. In this paper, and for the purpose of modeling shearlet subband dependences, we consider the use of subband energies to represent each shearlet subband. In our proposed approach, we employ two widely-used energy features, namely the norm-1 energy and the norm-2 energy, to represent each shearlet subband. To this end, we first perform an L-level shearlet transform on a given texture, and obtain one low-pass shearlet subband and M directional subbands at each scale. Then, for each shearlet subband denoted as $S = \{z_\tau\}_{\tau=1}^{N}$ we denote the modulus of the coefficient z_τ using $|z_\tau|$, and define the norm-1 energy and norm-2 energy features as

$$e_1 = \frac{1}{N}\sum_{\tau=1}^{N}|z_\tau| \tag{1}$$

and

$$e_2 = \sqrt{\frac{1}{N}\sum_{\tau=1}^{N}|z_\tau|^2} \tag{2}$$

respectively.

In fact, from a statistical viewpoint, the norm-1 energy is the sample mean of the moduli of coefficients in S, while the norm-2 energy measures the sample standard deviation. In this way, these two energy features can be used to capture the visual information of the shearlet subband S, whether from a signal energy representation or from a statistical viewpoint.

Furthermore, for any given direction, we can obtain a norm-1 energy feature vector consisting of the norm-1 energy feature vector $E_1^j = (e_1^0, e_1^{1,j}, e_1^{2,j}, \ldots, e_1^{L,j})$, where $e_1^{i,j}$ denotes the norm-1 feature in the j-th directional subband at the i-th scale ($j = 1, 2, \ldots, M$, $i = 1, 2, \ldots, L$); e_1^0 denotes the norm-1 feature in the low-pass subband. For clarity, we denote E_1^j with $(e_1^{0,j}, e_1^{1,j}, \ldots, e_1^{L,j})$, where $e_1^{0,j} = e_1^0$ due to the low-pass subband containing the information for every direction.

Meanwhile, a norm-2 energy feature vector can be constructed as $E_2^j = (e_2^{0,j}, e_2^{1,j}, \ldots, e_2^{L,j})$ in the same way, where $e_2^{i,j}$ denotes the norm-2 feature in the j-th directional subband at the i-th scale; $e_2^{0,j} = e_2^0$ and e_2^0 is the norm-2 feature in the low-pass subband. In this way, 2M feature vectors $\{E_1^1, E_1^2, \ldots, E_1^M, E_2^1, E_2^2, \ldots, E_2^M\}$ can be obtained. For simplicity, we denote these feature vectors by

$$P^t = (p^{0,t}, p^{1,t}, \ldots, p^{L,t}) \tag{3}$$

where $t = 1, 2, \ldots, 2M$. In the next subsection, we study how to model the dependence of these features.

B. Linear Regression Model of Adjacent Shearlet Subbands

Regression is a tool used for studying the dependence of attributes. So we can investigate the dependences between adjacent shearlet subbands for each direction by considering the dependences of their corresponding features using a linear regression tool. Consider a given training texture dataset$\{I_{c,n}\}_{n=1}^{N_{tr}}$, where c is the class label with $c = 1, 2, \ldots, C$. When an L-level shearlet transform is performed on each of N_{tr} training texture in the c-th class, we can obtain $2M * N_{tr}$ feature vectors $Q_{c,n}^t = (q_{c,n}^{0,t}, q_{c,n}^{1,t}, \ldots, q_{c,n}^{L,t})$ with $n = 1, 2, \ldots, N_{tr}$ and $t = 1, 2, \ldots, 2M$. We next investigated the dependences between adjacent subbands for each direction by considering $\{(q_{c,n}^{i-1,t}, q_{c,n}^{i,t})\}_{n=1}^{N_{tr}}$. For simplicity, we denote $\{(q_{c,n}^{i-1,t}, q_{c,n}^{i,t})\}_{n=1}^{N_{tr}}$ by $\{(x_n, y_n)\}_{n=1}^{N_{tr}}$, which can obviously be considered as the points in a 2-D coordinate system. Now, we model $\{(x_n, y_n)\}_{n=1}^{N_{tr}}$ using a linear regression model with one predictor, which we represent with X, and one response variable, which we denote with Y. Then the samples $\{(x_n, y_n)\}_{n=1}^{N_{tr}}$ can be seen as the N_{tr} observations of (X, Y).

A simple linear regression model consists of the mean function and the variance function

$$E(Y|X = x) = \beta_0 + \beta_1 x \tag{4}$$

$$Var(Y|X = x) = \sigma^2 \tag{5}$$

where the parameters in the mean function are the intercept β_0 and the slope β_1. The variance function is assumed to be constant, with a positive value σ^2 that is usually unknown [47].

The parameters β_0 and β_1 can be estimated by using ordinary least squares (OLS), and their OLS estimates are the values that minimize the residual sum of squares (RSS) function, which is defined as

$$G(\beta_0, \beta_1) = \sum_{n=1}^{N_{tr}}(y_n - \beta_0 - \beta_1 x_n)^2. \tag{6}$$

Differentiate $G(\beta_0, \beta_1)$ with respect to β_0 and β_1, set the derivatives equal to 0, and then obtain

$$\frac{\partial G(\beta_0, \beta_1)}{\partial \beta_0} = -2\sum_{n=1}^{N_{tr}}(y_n - \beta_0 - \beta_1 x_n) = 0 \tag{7}$$

$$\frac{\partial G(\beta_0, \beta_1)}{\partial \beta_1} = -2\sum_{n=1}^{N_{tr}} x_n(y_n - \beta_0 - \beta_1 x_n) = 0. \tag{8}$$

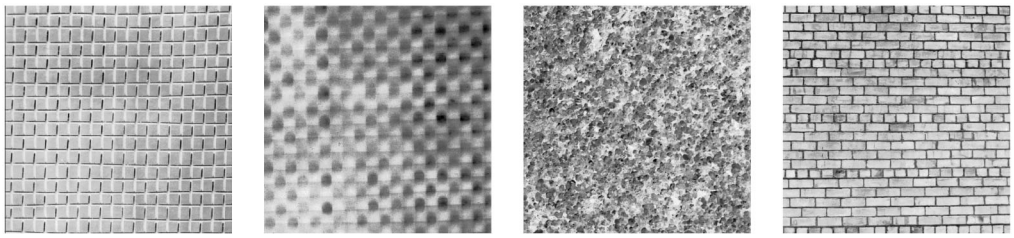

Fig. 2. Four texture classes. (a) D1. (b) D8. (c) D28. (d) D95.

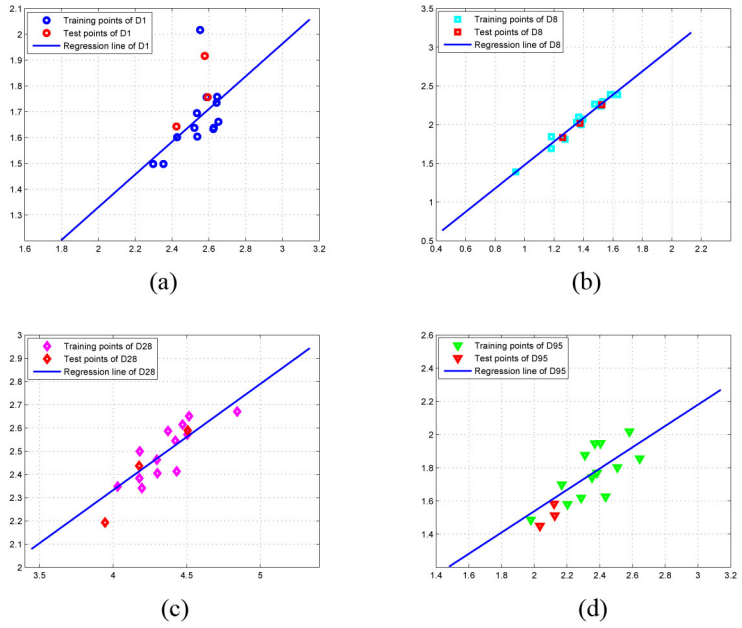

Fig. 3. Feature points obtained from the four texture classes D1, D8, D28, and D95 and the corresponding linear regression models. (a) D1. (b) D8. (c) D28. (d) D95.

By simply computing, we can obtain the OLS estimates of β_0 and β_1 as follows:

$$\hat{\beta}_0 = \bar{y} - \hat{\beta}_1 \bar{x}, \tag{9}$$

$$\hat{\beta}_1 = \frac{\sum_{n=1}^{N_{tr}} x_n y_n - N_{tr} \bar{x} \bar{y}}{\sum_{n=1}^{N_{tr}} x_n^2 - N_{tr} \bar{x}^2} \tag{10}$$

where $\bar{x} = \frac{1}{N_{tr}} \sum_{n=1}^{N_{tr}} x_n$, and $\bar{y} = \frac{1}{N_{tr}} \sum_{n=1}^{N_{tr}} y_n$.

We can obtain the regression coefficients in all the regression models used for modeling the dependences of all adjacent subband features in the same way as above. For clarity, Fig. 2 shows four Brodatz texture images D1, D8, D28, and D95, obtained from the Brodatz database [48] and used to represent four texture classes. We divide these four images into 16 texture patches, from which 13 patches are used as training samples and the others as test samples. For the purpose of modeling the dependences of shearlet subbands, we first perform a three-level shearlet decomposition with 10 directional subbands at each scale on each image patch. It should be obvious that $C = 4$, $N_{tr} = 13$, $M = 10$, and $L = 3$. We then construct the training feature vectors $Q_{c,n}^t$, and the test feature vectors (denoted by $\tilde{Q}_{c,n}^t = (\tilde{q}_{c,n}^{0,t}, \tilde{q}_{c,n}^{1,t}, \ldots, \tilde{q}_{c,n}^{L,t})$), of the c-th texture class.

In order to explain the linear regression models of adjacent shearlet subbands, Fig. 3(a) shows the 13 training feature points $\{(q_{c,n}^{i-1,t}, q_{c,n}^{i,t})\}_{n=1}^{13}$ and three test feature points $\{(\tilde{q}_{c,n}^{i-1,t}, \tilde{q}_{c,n}^{i,t})\}_{n=1}^{3}$ ($c = 1$, $i = 3$, and $t = 9$), where $c = 1$ denotes the texture class D1. Note that the 13 training feature points are marked by blue circles and the three test feature points by red circles. In addition, Fig. 3(a) also shows a regression straight line obtained from the training samples. Similarly, Fig. 3(b)–(d) shows the training and test feature points of D8, D28, and D95, as well as the corresponding regression straight lines. As we can see, for each texture class its test feature points almost follow the same linear regression relationship as its training feature points although there are two outliers for the D1 class. Fig. 4 shows the relations of the four regression straight lines in a common coordinate system. It can be seen from Fig. 4 that the test feature points of D8 are closer to the regression straight line obtained from the training feature points of D8, rather than the other three lines. Similar results can be observed for the texture class D28. Although the two texture classes D1 and D95 are very similar and almost homogeneous, only a small proportion of sample points of each class are far away from the regression line of the class to which they belong. Therefore, it is

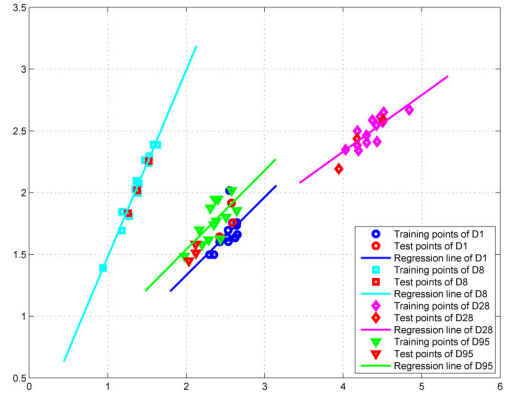

Fig. 4. Relations of the four linear regression straight lines corresponding to the four texture classes D1, D8, D28, and D95.

reasonable to utilize the linear regression approach to model the dependences of the adjacent shearlet subbands for texture classification.

In the next subsection, the distance from a test texture to all texture classes will be given.

C. Residual Analysis and Similarity Measurement

Once all the regression coefficients in the linear regression models are obtained for every texture, the response value of a test feature point with its estimated value obtained from the regression model can be compared using a metric. Given a test image I we can obtain $2M$ feature vectors $\{(p^{0,t}, p^{1,t}, \ldots, p^{L,t})\}_{t=1}^{2M}$ by means of the above feature extraction method. To define a distance from the test image I to the c-th texture class T_c, we consider the i-th pair of adjacent features $(p^{i-1,t}, p^{i,t})$ of the t-th vector and further utilize the corresponding regression coefficients $\{\hat{\beta}_0^{c,i,t}, \hat{\beta}_1^{c,i,t}\}$ of the c-th class to compute the residual $d_c^{i,t}$

$$d_c^{i,t} = \left| p^{i,t} - \hat{p}^{i,t} \right| \tag{11}$$

where

$$\hat{p}^{i,t} = E(Y|X = p^{i-1,t}) = \hat{\beta}_0^{c,i,t} + \hat{\beta}_1^{c,i,t} p^{i-1,t} \tag{12}$$

and $i = 1, 2, \ldots, L$. It follows that we can define the weighted summation of residuals (WSR) as the distance from the test image I to the c-th class T_c, which is given by:

$$D_{WSR}(I, T_c) = \sum_{t=1}^{2M} \sum_{i=1}^{L} 2^i d_c^{i,t}. \tag{13}$$

Note that the weight 2^i depends on the shearlet decomposition scale index i and is used for balancing the energy differences of shearlet subbands at different scales. After all the distances $\{D_{WSR}(I, T_c)\}_{c=1}^{C}$ between the test sample and the C texture classes are computed by formula (13), the test sample is assigned to the texture class corresponding to the minimum of $\{D_{WSR}(I, T_c)\}_{c=1}^{C}$.

Except for the scatterplots in Figs. 3 and 4, we further explain the rationality of this linear regression modeling assumption from the view of the similarity measurement defined by regression residuals. Instead of the four textures used in the previous subsection, we here use a large set of 40 640×640 texture images (shown in Fig. 5) from the Brodatz database [48]. In this experiment, each image is divided into 16 160×160 nonoverlapping patches. We select eight training samples from each of 40 classes and leave the remaining samples for testing. In the interest of saving space, we only investigate the similarity measurements from the texture samples of the D1 and D3 classes to the 40 texture classes, which are given in Tables I and II. Table I shows the values of the similarity measure $D_{WSR}(I, T_c)$ from the texture samples of the D1 class to all the 40 texture classes. It can be seen clearly that the distance from each sample of the D1 class to the D1 class is minimum among the distances from it to each of 40 texture classes. Furthermore, it is obvious that the average distance from training samples of D1 to the D1 class is less than that from testing samples of D1 to the D1 class. The similar results can be observed in Table II, which shows the values of the similarity measure $D_{WSR}(I, T_c)$ from the texture samples of the D3 class to all the 40 texture classes. These provide a sufficient verification for the rationality of this linear regression modeling assumption.

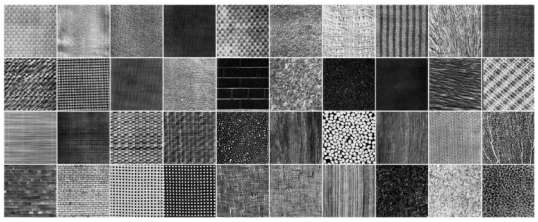

Fig. 5. Forty Brodatz texture images. From left to right and top to bottom: D1, D3, D4, D6, D8, D9, D10, D11, D15, D17, D18, D20, D21, D22, D25, D28, D33, D34, D37, D46, D49, D52, D56, D64, D66, D68, D75, D79, D82, D87, D94, D95, D101, D102, D103, D104, D106, D109, D110, and D111.

IV. Texture Retrieval Based on Linear Regression Modeling

Given a query texture and a dataset Ω consisting of N_{total} texture images from C texture classes, texture retrieval is used to pick out the relevant textures from the dataset Ω. In this section, we present a novel texture retrieval method with pseudo-feedback based on linear regression models of adjacent shearlet subband dependences. We first describe the framework of this texture retrieval method and then present a preretrieval approach based on contourlets.

A. Texture Retrieval With Pseudo-Feedback Based on Linear Regression Models

To perform texture retrieval with pseudo feedback, we need a texture retrieval method to preprocess the textures in Ω. In fact, any distance-based texture retrieval method can be used as the preprocessing step of our proposed texture retrieval method. Here, we assume that a preretrieval method has been performed on the dataset Ω. We then pick out a subset Ω_1 ($\Omega_1 \subseteq \Omega$) consisting of N_{top} ($N_{\text{top}} \leq N_{\text{total}}$) top-ranked textures. Generally speaking, the subset Ω_1 includes all relevant textures with the query texture; it is true that in the extreme

TABLE I
VALUES OF THE SIMILARITY MEASURE $D_{WSR}(I, T_c)$ $(\times 10^2)$ FROM THE 16 TEXTURE PATCHES OF THE D1 CLASS TO ALL THE 40 TEXTURE CLASSES

	Training texture patches								Testing texture patches							
	1	2	3	4	5	6	7	8	9	10	11	12	13	14	15	16
D1	**0.6**	**0.3**	**0.2**	**0.3**	**0.2**	**0.2**	**0.6**	**0.5**	**0.9**	**0.8**	**1.0**	**0.6**	**0.8**	**0.7**	**1.0**	**0.8**
D3	8.0	7.9	7.7	7.7	7.6	7.6	7.5	7.6	7.6	7.3	6.9	7.6	7.3	7.2	6.9	7.5
D4	14.0	13.8	13.6	13.4	13.4	13.4	13.1	12.7	14.0	14.1	13.0	12.8	13.7	14.0	13.0	12.6
D6	8.7	8.9	8.7	8.7	8.5	8.7	8.3	8.2	8.9	9.0	8.4	8.1	8.7	9.1	8.4	8.0
D8	8.1	9.3	8.8	9.3	8.6	9.0	8.5	9.1	8.3	8.6	8.0	8.7	8.7	8.7	8.3	9.0
D9	6.4	6.6	6.2	6.4	6.3	6.3	6.0	6.1	6.2	6.0	5.5	6.0	6.0	6.0	5.5	6.0
D10	5.4	5.4	5.2	5.4	5.0	5.2	5.2	5.6	4.6	4.4	4.3	5.6	4.5	4.3	4.4	5.6
D11	6.8	6.6	6.3	6.2	6.5	6.2	5.9	5.8	6.7	6.6	6.0	5.8	6.5	6.7	6.0	5.7
D15	4.6	3.8	3.9	4.0	4.5	4.0	3.9	3.9	4.5	3.9	3.9	4.0	4.6	4.2	4.0	4.0
D17	9.6	9.0	8.7	8.8	9.4	8.7	8.3	8.2	9.7	9.0	8.2	8.1	9.3	8.9	8.3	8.0
D18	3.9	3.2	3.2	3.1	3.9	3.1	3.2	3.1	3.8	3.2	3.6	3.2	4.0	3.4	3.6	3.2
D20	5.0	5.2	5.3	5.2	4.9	5.2	5.0	5.0	4.9	5.1	5.0	5.0	4.9	5.3	5.1	5.0
D21	12.9	13.6	13.0	13.4	13.0	13.3	12.9	13.2	13.1	13.1	12.3	13.0	12.7	12.8	12.3	12.9
D22	4.8	4.6	4.4	4.5	4.3	4.5	4.6	4.7	4.0	3.8	3.9	4.9	3.9	3.8	4.0	4.8
D25	4.3	4.0	3.6	3.9	4.4	3.9	3.4	3.8	4.4	3.6	3.2	3.6	4.3	3.6	3.3	3.7
D28	3.8	3.1	3.0	3.1	3.6	3.0	3.0	3.0	3.7	3.3	3.0	3.1	3.8	3.4	3.2	3.1
D33	5.0	4.5	4.3	4.4	4.8	4.3	4.0	4.0	5.0	4.4	4.1	3.9	5.0	4.5	4.1	3.9
D34	9.3	8.7	8.5	8.6	9.3	8.5	7.9	7.9	9.8	9.0	8.1	7.7	9.6	9.1	8.1	7.6
D37	4.9	5.4	5.0	5.2	4.9	5.2	4.8	4.9	5.4	5.4	4.5	4.7	5.0	5.3	4.4	4.6
D46	2.9	3.2	3.2	3.2	3.1	3.2	3.2	3.2	3.1	3.5	3.6	3.2	3.5	3.6	3.7	3.5
D49	15.5	14.4	14.3	14.3	15.1	14.3	14.4	14.5	14.7	13.9	14.3	14.3	14.3	13.5	13.8	14.1
D52	8.4	7.7	7.7	7.6	8.5	7.7	7.3	7.1	9.1	8.5	8.1	7.1	9.1	8.7	7.9	6.9
D56	3.1	2.3	2.4	2.2	3.0	2.3	2.4	2.2	3.0	2.5	2.8	2.2	3.1	2.7	2.6	2.2
D64	3.7	3.4	3.2	3.1	3.3	3.0	3.0	2.7	3.4	3.3	3.2	2.6	3.1	3.1	2.9	2.3
D66	4.9	4.1	4.0	4.1	5.0	4.1	3.8	3.8	5.2	4.3	4.0	3.8	5.2	4.5	4.1	3.8
D68	5.9	5.1	5.1	5.1	5.7	5.1	4.8	4.9	5.5	4.8	4.9	4.8	5.7	5.2	5.1	5.0
D75	3.0	2.3	2.5	2.4	3.0	2.4	2.5	2.4	3.0	2.6	2.9	2.5	3.2	2.7	2.9	2.5
D79	9.5	8.6	8.5	8.5	9.2	8.5	8.1	8.1	9.3	8.4	7.7	8.0	9.1	8.6	7.9	7.9
D82	5.2	5.1	4.7	4.9	5.0	4.7	4.5	4.6	4.8	4.3	3.9	4.5	4.7	4.4	4.1	4.5
D87	6.5	6.3	6.3	6.3	6.4	6.4	6.3	6.3	6.6	6.4	6.3	6.4	6.5	6.3	6.3	6.2
D94	3.4	3.1	2.7	2.9	3.4	2.9	2.6	2.7	3.7	3.0	2.3	2.6	3.5	2.8	2.3	2.5
D95	2.5	1.4	1.3	1.4	2.2	1.5	1.4	1.4	2.4	1.5	1.4	1.7	2.2	1.5	1.4	1.7
D101	5.5	5.1	5.2	5.2	5.4	5.1	5.1	5.0	5.8	5.4	5.1	5.1	5.8	5.5	5.1	5.1
D102	4.5	4.3	4.4	4.3	4.5	4.3	4.2	4.1	4.8	4.4	4.2	4.2	4.9	4.6	4.3	4.2
D103	13.6	13.5	13.4	13.2	13.4	13.3	13.0	12.7	13.9	13.8	13.0	12.8	13.6	13.7	12.9	12.5
D104	8.3	8.1	8.0	8.0	8.1	8.0	7.9	8.0	8.2	7.9	7.5	8.0	7.9	7.7	7.4	7.8
D106	14.6	15.6	15.4	15.6	14.7	15.4	14.8	15.1	14.8	15.3	14.6	14.8	15.0	15.6	15.0	15.1
D109	9.8	9.8	9.6	9.7	9.8	9.6	9.1	9.0	10.2	10.1	9.1	8.8	10.1	10.1	9.2	8.7
D110	7.0	7.1	6.8	7.0	6.9	6.9	6.6	6.8	6.7	6.4	6.0	6.7	6.6	6.5	6.1	6.7
D111	5.2	4.9	4.7	4.8	5.0	4.7	4.4	4.4	5.2	4.7	4.1	4.3	5.0	4.7	4.1	4.3

TABLE II
VALUES OF THE SIMILARITY MEASURE $D_{WSR}(I, T_c)$ $(\times 10^2)$ FROM THE 16 TEXTURE PATCHES OF THE D3 CLASS TO ALL THE 40 TEXTURE CLASSES

	Training texture patches								Testing texture patches							
	1	2	3	4	5	6	7	8	9	10	11	12	13	14	15	16
D1	9.3	10.9	10.3	9.8	10.7	11.5	10.3	11.1	8.3	10.7	9.5	9.6	9.6	10.7	10.5	10.1
D3	**1.7**	**1.6**	**1.4**	**1.3**	**1.7**	**1.6**	**1.3**	**1.3**	**1.5**	**1.5**	**1.4**	**1.7**	**1.8**	**1.6**	**1.4**	**1.6**
D4	4.7	4.5	5.1	5.2	4.8	4.4	4.4	5.3	4.2	4.6	4.3	5.1	4.2	4.4	4.6	5.0
D6	9.4	10.1	9.5	9.0	9.9	9.8	10.0	9.5	9.1	10.1	9.6	9.4	10.0	10.1	9.9	9.3
D8	17.6	17.2	17.8	20.0	19.1	17.6	17.3	20.0	15.7	17.2	15.4	17.1	18.3	17.5	17.5	17.8
D9	6.1	5.2	4.9	5.4	6.6	5.2	5.0	6.0	5.1	4.9	3.9	4.6	6.3	5.4	5.3	5.3
D10	3.3	3.4	2.4	3.0	3.2	3.4	2.2	3.0	2.7	3.1	2.1	2.9	3.1	3.1	2.2	2.5
D11	6.9	5.7	6.7	7.2	7.4	5.9	6.7	7.5	5.9	6.2	5.6	6.6	6.8	6.1	6.4	6.7
D15	5.9	6.3	5.4	6.4	5.6	6.7	5.3	6.3	5.7	6.4	5.5	6.2	6.1	6.3	4.9	5.8
D17	6.5	6.7	6.4	5.2	6.2	6.5	6.8	6.1	6.3	6.8	7.1	6.7	6.3	6.7	6.9	6.3
D18	6.2	6.6	6.6	6.7	6.3	7.2	6.6	7.2	5.9	6.7	6.5	7.1	6.6	6.6	6.4	6.8
D20	6.9	7.3	7.3	7.6	6.8	7.5	7.5	7.5	6.8	7.5	7.3	7.6	6.9	7.3	7.0	6.9
D21	14.7	15.9	17.0	15.7	17.2	17.2	16.7	17.1	14.4	16.2	15.7	15.6	15.9	16.5	16.7	16.2
D22	4.2	4.4	3.4	3.9	3.7	4.5	3.8	3.8	3.5	4.2	3.8	4.1	4.1	4.3	3.6	3.8
D25	6.5	7.3	7.5	8.2	7.1	7.0	6.8	8.0	5.9	7.1	5.7	6.5	6.8	7.3	6.7	6.9
D28	8.4	8.8	7.8	8.7	8.3	9.0	7.8	9.0	7.2	9.0	7.1	8.0	8.0	8.8	7.4	7.8
D33	4.3	4.5	3.8	3.6	4.0	4.2	3.7	4.0	4.0	4.4	3.8	4.4	4.4	4.3	3.7	3.9
D34	7.2	7.1	7.7	6.8	7.5	7.1	8.1	7.2	7.7	7.3	8.1	8.4	7.5	7.2	8.1	7.9
D37	7.8	7.8	8.4	8.4	8.6	8.3	8.2	8.7	7.3	7.8	7.9	7.9	7.3	7.5	8.2	7.4
D46	11.1	11.1	10.9	11.5	11.0	11.4	11.1	11.8	10.2	11.4	10.7	11.3	10.4	11.2	10.9	10.7
D49	16.4	18.5	19.2	17.1	17.7	19.1	19.0	18.0	16.9	18.6	19.0	17.8	17.6	18.9	19.0	18.4
D52	7.2	7.9	7.9	6.8	6.7	7.1	7.9	6.4	7.7	7.2	8.3	8.1	6.4	7.1	7.8	6.9
D56	8.2	9.0	9.1	9.2	8.7	9.6	8.8	9.5	7.7	9.2	8.4	8.7	8.8	9.3	8.6	8.7
D64	6.9	7.3	7.5	7.7	6.5	7.4	7.1	7.6	6.4	7.4	7.0	7.4	6.4	7.1	6.8	6.6
D66	8.0	8.8	9.0	8.5	8.3	9.0	9.0	9.0	7.5	8.9	8.4	8.7	7.7	8.8	8.9	8.5
D68	7.1	6.2	6.2	7.0	6.7	6.2	6.0	7.1	5.9	6.2	5.4	6.6	7.1	6.7	6.2	6.7
D75	7.2	7.6	7.5	8.0	7.3	8.0	7.3	8.2	6.6	7.9	7.0	7.7	7.2	7.6	7.0	7.5
D79	7.5	6.7	7.1	8.4	7.8	7.7	7.4	9.0	7.2	7.6	7.2	8.3	8.6	7.8	7.3	8.5
D82	6.3	5.4	5.2	6.4	7.3	5.9	5.0	7.4	5.2	5.3	4.4	5.9	7.0	5.8	5.2	6.3
D87	5.0	5.6	5.4	5.3	4.4	5.7	5.4	5.4	5.0	5.5	5.8	5.6	4.6	5.1	5.3	5.0
D94	6.2	6.9	7.1	7.2	6.9	7.3	6.7	7.3	5.7	6.6	6.5	6.5	6.0	6.6	6.8	6.1
D95	9.7	10.6	10.8	11.0	9.9	10.9	10.7	11.3	8.8	10.7	10.2	10.4	9.4	10.4	10.5	10.1
D101	6.2	6.1	5.9	6.1	5.8	6.3	6.1	6.4	5.5	6.4	6.2	6.1	5.9	6.0	5.7	5.9
D102	6.8	7.3	7.1	6.2	7.1	7.5	7.4	6.7	6.4	7.5	7.1	7.1	6.6	7.3	7.1	6.7
D103	7.5	8.4	8.5	7.0	6.9	8.1	9.1	7.1	8.5	8.3	9.7	8.9	7.4	8.2	8.7	8.0
D104	5.9	7.2	7.6	6.6	5.8	7.4	7.8	6.3	6.5	7.0	8.1	7.2	5.9	7.0	7.5	6.8
D106	17.6	16.9	17.5	19.2	17.5	17.0	16.9	18.4	16.5	16.9	16.2	17.4	17.8	17.0	17.0	17.3
D109	7.6	6.7	7.5	7.2	7.8	6.3	7.7	7.4	7.6	6.3	7.6	7.7	7.9	6.7	7.9	7.5
D110	4.6	3.6	4.6	5.1	5.4	4.0	4.2	5.2	4.2	3.4	3.2	4.4	5.5	4.0	4.6	4.8
D111	3.4	3.4	3.1	3.1	3.5	3.6	2.9	3.6	3.2	3.4	2.7	3.7	3.5	3.4	2.9	3.3

case $\Omega_1 = \Omega$, and we only select Ω_1 ($\Omega_1 \subset \Omega$) for the purpose of reducing the computational cost of texture retrieval. Note that for any given query texture the number of relevant textures in the dataset Ω is a fixed number, albeit previously unknown. For clarity, we denote the number of relevant textures in the dataset Ω by N_{rel}. So, the range of N_{top} should be $N_{\text{rel}} < N_{\text{top}} \leq N_{\text{total}}$.

In this way, the original texture retrieval problem is reduced to a simpler one retrieving N_{rel} relevant textures from Ω_1 consisting of N_{top} textures. To this end, we need to perform a shearlet transform to each texture in Ω_1 and extract the energy features to represent the shearlet subband. We then select N_{reg} ($2 \leq N_{\text{reg}} \leq N_{\text{rel}}$) texture images from Ω_1 to construct linear regression models using their energy features and estimate

TABLE III
PROCEDURE OF OUR PROPOSED TEXTURE RETRIEVAL METHOD USING THE PSEUDO-FEEDBACK MECHANISM BASED ON LINEAR REGRESSION

[Input:] A texture image dataset and a query.
[Output:] The N_{rel} retrieved texture images.

1) Rank the texture image by using a preprocessing retrieval method.
2) Select N_{reg} $(2 \leq N_{reg} \leq N_{rel})$ top ranked textures as the relevant textures of the query used for linear regression modeling
3) Perform the shearlet transform on all the N_{top} $(N_{reg} < N_{top} \leq N_{total})$ top ranked textures.
4) Extract the energy features from each shearlet subband by Eqs. (1) and (2).
5) According to Eqs. (9) and (10), compute the estimated parameter values of the linear regression models on the corresponding directional subbands of the N_{reg} relevant textures.
6) Compute the distances from each of the rest N_{top}-N_{reg} textures to the texture class in which the query texture belongs using Eq. (13).
7) Rank the N_{top}-N_{reg} textures and obtain the N_{rel}-N_{reg} top ranked textures.
8) Return the N_{rel} retrieved textures.

the model parameters. Note that we let $N_{\text{reg}} = [N_{\text{rel}}/2]$ in our experiments. In fact, if too few samples (e.g., $N_{\text{reg}} = 2$) are selected for constructing linear regression straight lines, the resulting lines may be far away from the true regression lines of all the relevant samples. In contrast, if too many samples (e.g., $N_{\text{reg}} = N_{\text{rel}} - 1$) are selected as relevant samples for constructing linear regression straight lines, the number of the remaining relevant samples in Ω_1 is too small, and thus the pseudo-feedback will have almost no effect on the retrieval result obtained by the preretrieval method. When we compute the distances from each of the remaining $N_{\text{top}} - N_{\text{reg}}$ textures to the class in which the query texture belongs, we can obtain the $N_{\text{rel}} - N_{\text{reg}}$ top-ranked textures according to these distances. Finally, we can obtain the N_{rel} retrieved textures consisting of the $N_{\text{rel}} - N_{\text{reg}}$ top ranked textures and the previously assumed relevant N_{reg} textures with the query. Table III shows the procedure of our proposed texture retrieval method using the pseudo-feedback mechanism based on linear regression.

Note that the rationale for performing the second retrieval is as follows. Consider that, for the queried images using the first retrieval, the top-ranked images are more similar to the query image than the other images, and thus the N_{reg} top-ranked images in the queried images are regarded as images with the same class label as the query. Therefore, the retrieval problem can be considered as a two-class classification, that is, the textures whose energy features are close to the linear regression straight lines belong to the class that the query belongs to, and the others belong to another class. We can therefore adjust the first retrieval result by using the pseudo-feedback mechanism based on the linear regression models.

B. Preretrieval Based on Statistical Contourlet Subband Characterization

In this subsection, we present a contourlet-based texture retrieval method for preretrieval. For the details of this method, see Reference [42].

1) Statistical Contourlet Subband Characterization: In this contourlet-based texture retrieval approach, we use six statistics to describe the probability density function [*pdf*, denoted by $g(x)$] of the coefficients in each contourlet subband. In particular, for the j-th directional subband at the i-th scale ($j = 1, 2, \ldots, M_{\text{con}}$, $i = 1, 2, \ldots, L_{\text{con}}$)[1] we let $\bar{\omega}_{N_{i,j}} = \frac{1}{N_{i,j}} \sum_{\tau=1}^{N_{i,j}} \omega_\tau$, and $S^l_{N_{i,j}} = \frac{1}{N_{i,j}} \sum_{\tau=1}^{N_{i,j}} (\omega_\tau - \bar{\omega}_{N_{i,j}})^l$, $l = 2, \ldots, 4$, $\omega_\tau \in V_{i,j}$, $V_{i,j}$ is the set consisting of the absolute coefficients in the j-th directional subband at the i-th scale, and $N_{i,j}$ is the number of coefficients in $V_{i,j}$. The six statistics are then given as follows.

1) Sample mean (one-order origin moment): $f_1^{i,j} = \bar{\omega}_{N_{i,j}}$.
2) Median (one-order): $f_2^{i,j} = \frac{1}{2}\left(\tilde{\omega}_{\frac{N_{i,j}}{2}} + \tilde{\omega}_{\frac{N_{i,j}}{2}+1}\right)$ if $N_{i,j}$ is even, $= \tilde{\omega}_{\frac{N_{i,j}+1}{2}}$ otherwise, where $\tilde{\omega}_n$ is the n-th order statistic from the sample $V_{i,j}$.
3) Sample variance (two-order central moment): $f_3^{i,j} = S^2_{N_{i,j}}$.
4) Norm-2 energy (two-order origin moment): $f_4^{i,j} = \frac{1}{N_{i,j}} \sum_{\tau=1}^{N_{i,j}} \omega_\tau^2$.
5) Absolute skewness: $f_5^{i,j} = \left| \frac{S^3_{N_{i,j}}}{(S^2_{N_{i,j}})^{3/2}} \right|$.
6) Kurtosis: $f_6^{i,j} = \frac{S^4_{N_{i,j}}}{(S^2_{N_{i,j}})^2}$.

Note that the absolute skewness measures the lack of symmetry in the *pdf* $g(x)$, while the kurtosis measures the flatness of the *pdf* $g(x)$. For the low-pass subband, these six statistics can be computed in the same manner as above, and are denoted by f_k^0 with $k = 1, 2, \ldots, 6$.

Considering the j-th directional information of one texture, we find that the low-pass subband contains some information about the j-th direction of one texture, in addition to the j-th directional subbands at different scales. We therefore construct the following six directional feature vectors (DFVs) to represent the j-th directional information of the texture:

$$F_k^j = \left(f_k^{0,j}, f_k^{1,j}, \ldots, f_k^{L_{\text{con}},j}\right) \tag{14}$$

where $f_k^{0,j} = f_k^0$, $j = 1, 2, \ldots, M_{\text{con}}$ and $k = 1, 2, \ldots, 6$. That is, F_k^j represents the DFV that consists of the k-th statistics from the j-th directional suband at all the L_{con} scales, as well as the low-pass subband. In this way, a texture can be characterized by these $6M_{\text{con}}$ DFVs, and we can distinguish two textures from their DFVs according to some discrepancy measurement.

2) Discrepancy Measurement and Texture Retrieval: After all DFVs are obtained for a query image and every texture image in a given dataset, retrieval requires that DFVs are compared to measure the distance between the query image and every candidate texture image. Since the six DFVs in each contourlet subband each have their own metric units, in order to make a uniform measure for them we employ a $Relative - L_1$ (RL_1) distance as our discrepancy metric of two DFVs F_k^j and $\tilde{F}_k^j$. Specifically, the RL_1 distance is a weighted

[1]To differentiate from the number M of directional subbands and the number L of decomposition scales in the shearlet transform, we use M_{con} and L_{con} as the corresponding values in the contourlet transform.

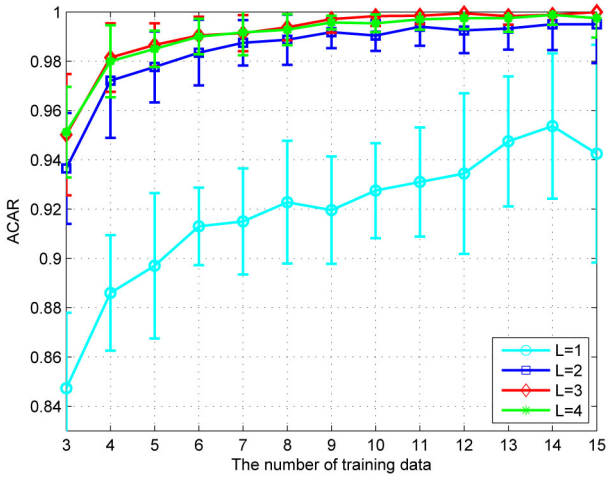

Fig. 6. Average classification accuracy rates of our proposed method with respect to the number of training samples in the four cases of the decomposition scale number.

L_1 distance and expressed as follows:

$$RL_1(F_k^j, \tilde{F}_k^j) = \sum_{i=0}^{L_{con}} \frac{\left| f_k^{i,j} - \tilde{f}_k^{i,j} \right|}{1 + f_k^{i,j} + \tilde{f}_k^{i,j}} \tag{15}$$

where $F_k^j = (f_k^{0,j}, f_k^{1,j}, \ldots, f_k^{L_{con},j})$ and $\tilde{F}_k^j = (\tilde{f}_k^{0,j}, \tilde{f}_k^{1,j}, \ldots, \tilde{f}_k^{L_{\text{con}},j})$.

For two given texture images I_1 and I_2, we can obtain one low-pass subband and M_{con}-directional subbands at each scale after having implemented an L_{con}-level contourlet transform on them, and then define the distance between the two texture images by the summation of RL_1s (abbreviated as SRL)

$$D_{\text{SRL}}(I_1, I_2) = \sum_{k=1}^{6} \sum_{j=1}^{M_{\text{con}}} RL_1\left(F_k^j, \tilde{F}_k^j\right) \tag{16}$$

where F_k^j and $\tilde{F}_k^j$ are the k-th DFVs representing the j-th directional information of the two images I_1 and I_2, respectively.

In this way, the distances between the query image and every candidate image can be computed by D_{SRL}. We can then sort these distances in increasing order and pick out the set of closest images to the first retrieval result, which is followed by the second retrieval using the pseudo-feedback mechanism based on linear regression as proposed in the previous subsection.

V. Experiment Results

Here, we perform various experiments to demonstrate the efficiency of our proposed texture classification and retrieval methods. For these experiments, we select the Laplacian pyramid filter by the 9–7 filters in the shearlet transform, which are the biorthogonal wavelet filters. In addition, we impose that each image is decomposed into one low-pass subband and 10 directional subbands at each scale. It therefore follows that $M = 10$.

A. Texture Classification

For clarity, we refer to our proposed texture classification method based on linear regression modeling of shearlet subband dependences and the minimum distance classifier as LRS-MD.

1) Classification Performance Evaluation: In this subsection, we evaluate our method of texture classification on the typical set of 40 640 × 640 Brodatz texture images shown in Fig. 5 (denoted by Set-1). In this experiment, each image is divided into 16 160 × 160 nonoverlapping patches, and thus there are 640 samples available in total. We select N_{tr} training samples from each of 40 classes and leave the remaining samples for testing with $N_{tr} = 3, 4, \ldots, 15$. Furthermore, the partitions are randomly obtained and the average classification accuracy rate (ACAR) is computed over the experiment results using 10 random splits of the training and test sets. In the following experiments, the ACAR is always defined in the same way.

We first investigate the sensitivity of decomposition scale to classification performance. Fig. 6 shows the ACAR of LRS-MD with respect to the number of training samples. It can be seen that the ACARs of LRS-MD with any given decomposition scale increase almost monotonically with the number of training samples. The ACARs of LRS-MD with $L = 3$ outperforms those with $L = 1$, 2, and 4. The error bars are also plotted in Fig. 6, where each error bar represents the standard deviation of the ACAR. The average of error bars of LRS-MD with $L = 3$ are notably smaller than those with $L = 1$, 2, and 4. This implies that the optimal number L of decomposition scales should be 3.

We further evaluate our proposed method by comparing it with three recently developed methods. The first method is based on the BP-P model and minimum distance classifier (BP-MD), proposed in [31]. The second is the method using the c-means clustering in the contourlet domain and the K-nearest neighbor (KNN) classifier (MCC-KNN), proposed in [40]. The third is the method based on the Poisson mixtures in the contourlet domains and the Bayesian classifier (PMC-BC), proposed in [41]. The second column of Table IV reports the ACARs of the four texture classification methods performed on Set-1 in the case of eight training samples. As seen in the second column, the ACAR of our proposed LRS-MD is higher than the other three methods by over 1.66%, and its standard deviation is visibly less than the other three methods.

2) Comparison Using Larger Brodatz Datasets: To further demonstrate the efficiency of LRS-MD, we use two larger Brodatz texture datasets and compare LRS-MD with the three texture classification methods presented above. The first large dataset consists of 60 Brodatz texture images, denoted by Set-2.[2] The second large data set is the whole Brodatz texture dataset, consisting of 111 texture images, and denoted by Set-3. All the texture images in these two datasets are of size 640 × 640, and each is divided into 16 160 × 160 nonoverlapping patches. Thus, there are 960 and 1776 samples available in total, respectively. Eight texture patches in each class are selected for training, and the other patches in each class are used for testing. The ACARs of these methods are listed in

[2] Set-2 (60 Classes) consisting of the 40 classes in Set-1 and the following 20 classes: D5, D16, D19, D26, D29, D32, D35, D47, D48, D53, D55, D57, D65, D67, D74, D76, D77, D80, D93, and D112.

TABLE IV
AVERAGE CLASSIFICATION ACCURACY RATES (ACARS, %) OF BP-MD, MCC-KNN, PMC-BC, AND LRS-MD ON THE FIVE DATASETS IN THE CASE OF EIGHT-TRAINING SAMPLES

Methods	Set-1	Set-2	Set-3	Set-4	Set-5
BP-MD [31]	94.87 ± 0.92	93.88 ± 1.13	78.77 ± 2.18	84.44 ± 1.65	80.58 ± 1.23
MCC-KNN [40]	97.03 ± 0.86	95.42 ± 1.23	75.73 ± 1.07	79.47 ± 1.89	72.25 ± 1.77
PMC-BC [41]	97.72 ± 0.61	98.15 ± 0.53	87.03 ± 1.35	92.31 ± 1.69	87.52 ± 2.33
LRS-MD	99.38 ± 0.53	99.27 ± 0.52	90.09 ± 1.71	97.44 ± 0.92	93.23 ± 1.53

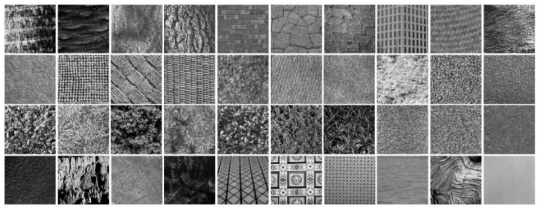

Fig. 7. Forty VisTex texture images.

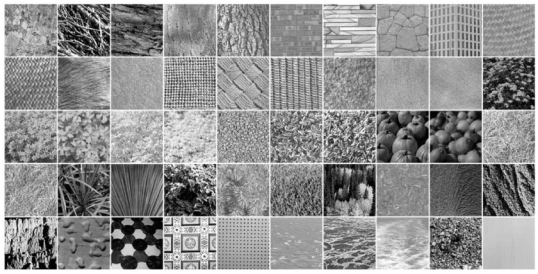

Fig. 8. Fifty VisTex texture images.

Table IV. It can be seen that LRS-MD outperforms BP-MD, MCC-KNN, and PMC-BC by over 1.12% on these two large Brodatz datasets.

3) Comparison Using VisTex Datasets: In this subsection, we further compare our method with BP-MD, MCC-KNN, and PMC-BC using two datasets from the VisTex database [49]. The first is the dataset consisting of 40 512×512 VisTex texture images (denoted by Set-4, and shown in Fig. 7). The second consists of 50 VisTex texture images (denoted by Set-5, and shown in Fig. 8). Each image is divided into 16 128×128 nonoverlapping patches, and thus there are 640 and 800 samples available in total, respectively. Eight texture patches in each class are selected for training, and the other patches in each class are used for testing. The ACARs of these methods are listed in Table IV. It can be seen that LRS-MD outperforms BP-MD, MCC-KNN, and PMC-MD by over 5.13% on these two VisTex datasets.

For a more intensive comparison with BP-MD, MCC-KNN, and PMC-MD, the classification accuracy rates of all 50 texture classes in Set-5 are shown in Table V. It can be seen that our method does not perform worse than the other three methods for 39 texture classes. Our method delivers 100% classification accuracy rate for 24 texture classes, compared to a maximum of 11 texture classes recognized without error by the other methods. The worst classification accuracy rates of the four methods, BP-MD, MCC-KNN, PMC-MD, and LRS-MD, are 16.25%, 15.00%, 31.25%, and 42.50%, respectively.

In summary, our proposed LRS-MD is efficient for performing texture classification and outperforms three state-of-the-art texture classification methods (BP-MD, MCC-KNN, and PMC-MD).

B. Texture Retrieval

For our texture retrieval experiments, the parameters used in the first texture retrieval based on statistical contourlet subband characterization are the same as the parameters given in [42].

1) Retrieval Performance Evaluation and Comparison: We first evaluate the efficiency of our proposed texture retrieval method on Set-1, consisting of 40 gray 640×640 images. In this experiment, each image is divided into 16 160×160 nonoverlapping patches, and thus there are 640 samples available in total. Any patch is selected as a query sample from each of the 40 classes, and the relevant samples for every query are defined as the other 15 samples from the same texture image; therefore, $N_{\text{rel}} = 15$. The retrieval performance is evaluated by the average retrieval rate (ARR), which is defined as the average percentage of number of relevant samples in the top 15 retrieved samples. In the following experiments, the relevant samples for every query and the ARR are defined in the same manner.

For the parameter N_{top} in the second retrieval phase, we let $N_{top} \in [3N_{\text{rel}}, 4N_{\text{rel}}]$. While we also consider other values of N_{top}, the experiment results reveal that the values of N_{top} in this interval are satisfactory. For example, the ARR of our proposed retrieval method on Set-1 is 96.27% in the case of $N_{\text{top}} = 3N_{\text{rel}} + N_{\text{reg}} = 3N_{\text{rel}} + [N_{\text{rel}}/2] = 52$. Although the ARR is 97.01% in the extreme case of $N_{\text{top}} = N_{\text{total}} = 600$, the computational cost of this case is nearly 10 times greater than that of the former in the second retrieval phase.

Next, we compare our proposed texture retrieval method with three current state-of-the-art texture retrieval approaches. The first one is the method based on the BP probability (BP-P; referred to as BPP), which was proposed in [33] and further improved on in [31]. The second is the method using the local energy histograms (LEH) [50]. The third retrieval method is based on statistics in the contourlet subbands (SCS) [42]. For clarity, we refer to the proposed retrieval method based on SCS and LRS-MD as SCS + LRS-MD. Table VI reports the ARRs of BPP, LEH, SCS, and our proposed SCS + LRS-MD. As can be seen from Table VI, SCS + LRS-MD outperforms BPP, LEH, and SCS by over 3.11%.

TABLE V
AVERAGE CLASSIFICATION ACCURACY RATE (ACAR, %) FOR EACH OF 50 TEXTURE CLASSES IN SET-5 WITH THE FOUR METHODS: COLUMN 1: BP-MD, COLUMN 2: MCC-KNN, COLUMN 3: PMC-BC, COLUMN 4: OUR PROPOSED LRS-MD

	1	2	3	4		1	2	3	4
Bark.0002	95.00	66.25	83.75	98.75	Food.0007	80.00	58.75	92.50	100
Bark.0003	68.75	53.75	92.50	100	Food.0008	73.75	80.00	100	100
Bark.0004	83.75	88.75	95.00	98.75	Food.0010	77.50	41.25	76.25	90.00
Bark.0008	47.50	46.25	73.75	82.50	Food.0011	100	83.75	88.75	100
Bark.0009	21.25	15.00	31.25	98.75	Grass.0001	67.50	40.00	75.00	70.00
Brick.0001	100	98.75	100	100	Grass.0002	75.00	60.00	81.25	62.50
Brick.0002	100	75.00	93.75	100	Leaves.0000	82.50	35.00	75.00	77.50
Brick.0004	100	93.75	93.75	100	Leaves.0002	87.50	96.25	90.00	98.75
Buildings.0009	100	86.25	93.75	100	Leaves.0005	16.25	55.00	33.75	80.00
Fabric.0000	80.00	97.50	97.50	100	Leaves.0010	62.50	37.50	95.00	68.75
Fabric.0002	75.00	81.25	81.25	96.25	Leaves.0013	77.50	95.00	87.50	98.75
Fabric.0004	90.00	100	91.25	93.75	Leaves.0015	48.75	32.50	75.00	75.00
Fabric.0007	92.50	97.50	100	100	Misc.0003	72.50	88.75	88.75	96.25
Fabric.0009	100	86.25	100	100	Sand.0004	78.75	100	88.75	100
Fabric.0011	85.00	78.75	96.25	100	Sand.0006	100	93.75	92.50	96.25
Fabric.0013	97.50	95.00	100	100	Stone.0001	78.75	68.75	87.50	100
Fabric.0015	98.75	88.75	98.75	100	Stone.0002	92.50	87.50	98.75	96.25
Fabric.0017	100	100	100	100	Tile.0003	83.75	47.50	72.50	100
Fabric.0018	100	100	100	100	Tile.0004	98.75	81.25	100	100
Flowers.0000	66.25	76.25	85.00	100	Tile.0007	98.75	87.50	87.50	100
Flowers.0002	55.00	70.00	80.00	85.00	Water.0002	88.75	60.00	81.25	91.25
Flowers.0003	100	36.25	83.75	88.75	Water.0004	73.75	83.75	97.50	98.75
Flowers.0004	78.75	46.25	97.50	98.75	Water.0007	81.25	82.50	93.75	90.00
Flowers.0005	86.25	73.75	90.00	87.50	WheresWaldo.0002	16.25	17.50	58.75	42.50
Food.0002	95.00	47.50	100	100	Wood.0002	100	100	100	100
					Mean	80.58	72.25	87.53	93.23

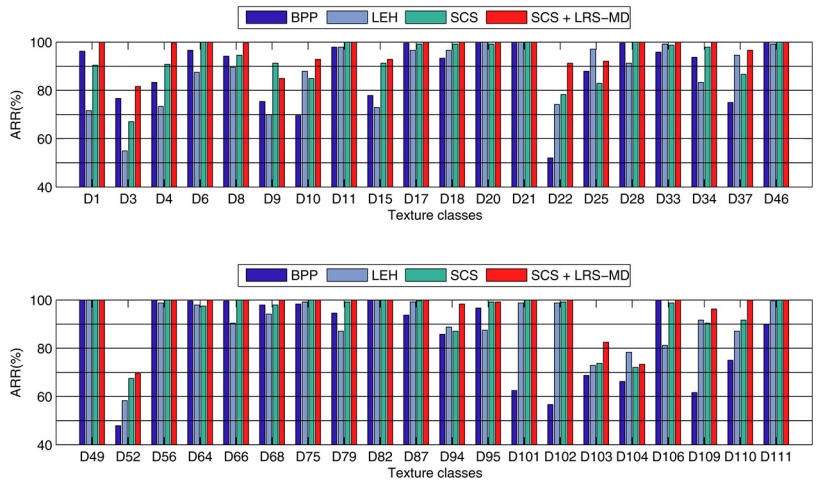

Fig. 9. Average retrieval rates (ARRs, %) of BPP, LEH, SCS, and our proposed SCS + LRS-MD for individual texture class of Set-1.

For an intensive comparison with BPP, LEH, and SCS, in Fig. 9 we summarize the retrieval rates of BPP, LEH, SCS, and our proposed SCS + LRS-MD for individual texture classes. We observe that SCS + LRS-MD either has equivalent ARRs or outperforms the other three methods for 37 texture classes, among which 25 texture classes can be retrieved by SCS + LRS-MD without error. Significantly, the retrieval rate of SCS + LRS-MD is equal to or greater than the retrieval rate of SCS for 39 texture classes, which verifies that our proposed pseudo-feedback mechanism based on linear regression modeling of dependences between shearlet subbands is effective. The minimum ARRs for the four methods (BPP, LEH, SCS, and our proposed SCS + LRS-MD) over all 40 classes are achieved on D52 (47.92%), D2 (55.00%), D2(67.08%), and D52 (69.58%), respectively. In other words, SCS + LRS-MD significantly outperforms these three methods on this dataset.

2) Further Comparison on Other Datasets: In this subsection, we demonstrate the use of SCS + LRS-MD on four other datasets (Set-2, Set-3, Set-4, and Set-5) and further compare with BPP, LEH, and SCS. Each texture in these four datasets is divided into 16 nonoverlapping patches in the same way as in the texture classification experiments. For each dataset, the query texture is selected in the same way as in the above subsection. Table VI reports the ARRs of BPP, LEH, SCS, and SCS + LRS-MD. As can be seen, SCS + LRS-MD outperforms the other three methods by over 3%.

To provide additional justification for the use of SCS + LRS-MD, we also compare it with the current state-of-the-art texture retrieval method based on the generalized gamma density (referred to as GD) method proposed in [51]. For convenience of comparison, we use the same dataset (Set-4) with

TABLE VI
AVERAGE RETRIEVAL RATES (ARRS, %) OF BPP, LEH, SCS, AND OUR PROPOSED SCS + LRS-MD ON THE FIVE TEXTURE DATASETS

Methods	Set-1	Set-2	Set-3	Set-4	Set-5
BPP [33]	86.50 ± 1.86	84.43 ± 1.78	66.16 ± 1.86	73.41 ± 3.30	66.60 ± 3.99
LEH [50]	88.69 ± 2.45	86.49 ± 2.59	69.75 ± 2.81	74.08 ± 3.41	67.18 ± 4.36
SCS [42]	93.16 ± 1.71	92.24 ± 1.61	75.30 ± 2.39	80.60 ± 3.02	71.55 ± 3.41
SCS + LRS-MD	96.27 ± 1.51	95.73 ± 1.70	80.15 ± 2.41	86.18 ± 2.94	78.93 ± 3.50

the same experimental setting as in [51]. The ARR of SCS + LRS-MD is 86.18%, which is obviously higher than that of GD, reported as 78.40% in [51].

In summary, our proposed SCS + LRS-MD outperforms four recently developed texture retrieval methods in five large datasets.

VI. CONCLUSION

Here, we present novel texture classification and retrieval methods in which shearlet subband dependences are modeled using linear regression. In order to overcome the inherent complexity of shearlet coefficients, we extract energy features from shearlet subbands and model their dependences using linear regression. The regression residuals are used for defining the distance from a test texture to a texture class. Our proposed texture retrieval method uses pseudo-feedback based on linear regression modeling to modify the retrieval result. Comprehensive experimentation in five large texture datasets reveals that our proposed classification and retrieval methods convincingly outperform the current state-of-the-art.

REFERENCES

[1] F. Lehmann, "Turbo segmentation of textured images," *IEEE Trans. Pattern Anal. Mach. Intell.*, vol. 33, no. 1, pp. 16–29, Jan. 2011.

[2] L. Liu and P. W. Fieguth, "Texture classification from random features," *IEEE Trans. Pattern Anal. Mach. Intell.*, vol. 34, no. 3, pp. 574–586, Mar. 2012.

[3] P. Arbelaez, M. Maire, C. Fowlkes, and J. Malik, "Contour detection and hierarchical image segmentation," *IEEE Trans. Pattern Anal. Mach. Intell.*, vol. 33, no. 5, pp. 898–916, May 2011.

[4] U. Kandaswamy, D. Adjeroh, S. Schuckers, and A. Hanbury, "Robust color texture features under varying illumination conditions," *IEEE Trans. Syst., Man, Cybern. B, Cybern.*, vol. 42, no. 1, pp. 58–68, Feb. 2012.

[5] B. S. Manjunathi and W. Y. Ma, "Texture features for browsing and retrieval of image data," *IEEE Trans. Pattern Anal. Mach. Intell.*, vol. 18, no. 8, pp. 837–842, Aug. 1996.

[6] S. Zhang, J. Huang, H. Li, and D. Metaxas, "Automatic image annotation and retrieval using group sparsity," *IEEE Trans. Syst., Man, Cybern. B, Cybern.*, vol. 42, no. 3, pp. 838–849, Jun. 2012.

[7] B. Leibe and B. Schiele, "Analyzing appearance and contour based methods for object categorization," in *Proc. IEEE CVPR*, 2003.

[8] Y. Xu *et al*., "Detection of sudden pedestrian crossings for driving assistance systems," *IEEE Trans. Syst., Man, Cybern. B, Cybern.*, vol. 42, no. 3, pp. 729–739, Jun. 2012.

[9] M. Hu, Y. Wang, Z. Zhang, D. Zhang, and J. Little, "Incremental learning for video-based gait recognition with LBP flow," *IEEE Trans. Cybern.*, vol. 43, no. 1, pp. 77–89, Feb. 2013.

[10] J. Shotton, J. Winn, C. Rother, and A. Criminisi, "Textonboost for image understanding: Multi-class object recognition and segmentation by jointly modeling texture, layout, and context," *Int. J. Comput. Vis.*, vol. 81, no. 1, pp. 2–23, 2009.

[11] E. Shahrian and D. Rajan, "Weighted color and texture sample selection for image matting," in *Proc. IEEE CVPR*, Providence, RI, USA, 2012, pp. 718–725.

[12] J. Zhang, M. Marszalek, S. Lazebnik, and C. Schmid, "Local features and kernels for classification of texture and object categories: A comprehensive study," *Int. J. Comput. Vis.*, vol. 73, no. 2, pp. 213–238, Feb. 2007.

[13] A. Bosch, A. Zisserman, and X. Muoz, "Scene classification using a hybrid generative/discriminative approach," *IEEE Trans. Pattern Anal. Mach. Intell.*, vol. 30, no. 4, pp. 712–727, Apr. 2008.

[14] L.-J. Li, R. Socher, and F.-F. Li, "Towards total scene understanding: Classification, annotation and segmentation in an automatic framework," in *Proc. IEEE CVPR*, 2009, pp. 2036–2043.

[15] J. R. Smith, C.-Y. Lin, and M. Naphade, "Video texture indexing using spatiotemporal wavelets," in *Proc. Int. Conf. Image Process.*, 2002, pp. 437–440.

[16] A. Ravichandran, R. Chaudhry, and R. Vidal, "Categorizing dynamic textures using a bag of dynamical systems," *IEEE Trans. Pattern Anal. Mach. Intell.*, vol. 35, no. 2, pp. 342–353, Feb. 2013.

[17] S. Dubois, R. Peteri, and M. Menard, "Decomposition of dynamic textures using morphological component analysis," *IEEE Trans. Circuits Syst. Video Technol.*, vol. 22, no. 2, pp. 188–201, Feb. 2012.

[18] Z. H. Guo, L. Zhang, and D. Zhang, "A completed modeling of local binary pattern operator for texture classification," *IEEE Trans. Image Process.*, vol. 19, no. 6, pp. 1657–1663, Jun. 2010.

[19] R. M. Haralick, K. Shanmugan, and I. Dinstein, "Texture features for image classification," *IEEE Trans. Syst., Man, Cybern.*, vol. 3, no. 6, pp. 610–621, Nov. 1973.

[20] T. H. Hong, C. R. Dyer, and A. Rosenfeld, "Texture primitive extraction using an edge-based approach," *IEEE Trans. Syst., Man, Cybern.*, vol. 10, no. 10, pp. 659–675, Oct. 1980.

[21] P. Garcia-Sevilla and M. Petrou, "Classification of binary textures using the 1-D Boolean model," *IEEE Trans. Image Process.*, vol. 8, no. 10, pp. 1457–1462, Oct. 1999.

[22] K. Zhan, J. Teng, and Y. Ma, "Spiking cortical model for rotation and scale invariant texture retrieval," *JIHMSP*, vol. 4, no. 3, pp. 155–165, Jul. 2013.

[23] A. Speis and G. Healey, "Feature extraction for texture discrimination via random field models with random spatial interaction," *IEEE Trans. Image Process.*, vol. 5, no. 4, pp. 635–645, Apr. 1996.

[24] S. Liao, M. W. K. Law, and A. C. S. Chung, "Dominant local binary patterns for texture classification," *IEEE Trans. Image Process.*, vol. 18, no. 5, pp. 1107–1118, May 2009.

[25] M. Unser, "Texture classification and segmentaion using wavelet frames," *IEEE Trans. Image Process.*, vol. 4, no. 11, pp. 1549–1560, Nov. 1995.

[26] T. Randen and J. H. Husoy, "Filtering for texture classification: A comparative study," *IEEE Trans. Pattern Anal. Mach. Intell.*, vol. 21, no. 4, pp. 291–310, Apr. 1999.

[27] G. V. D. Wouwer, P. Scheunders, and D. V. Dyck, "Statistical texture characterization from discrete wavelet representations," *IEEE Trans. Image Process.*, vol. 8, no. 4, pp. 592–598, Apr. 1999.

[28] S. C. Kim and T. J. Kang, "Texture classification and segmentation using wavelet packet frame and Gaussian mixture model," *Pattern Recognit.*, vol. 40, no. 4, pp. 1207–1221, Apr. 2007.

[29] S. Selvan and S. Ramakrishnan, "SVD-based modeling for image texture classification using wavelet transformation," *IEEE Trans. Image Process.*, vol. 16, no. 11, pp. 2688–2696, Nov. 2007.

[30] M. N. Do and M. Vetterli, "Wavelet-based texture retrieval using generalized Gaussian density and Kullback–Leibler distance," *IEEE Trans. Image Process.*, vol. 11, no. 2, pp. 146–158, Feb. 2002.

[31] S. K. Choy and C. S. Tong, "Statistical properties of bit-plane probability model and its application in supervised texture classification," *IEEE Trans. Image Process.*, vol. 17, no. 8, pp. 1399–1405, Aug. 2008.

[32] H. Lategahn, S. Gross, T. Stehle, and T. Aach, "Texture classification by modeling joint distributions of local patterns with Gaussian mixtures," *IEEE Trans. Image Process.*, vol. 19, no. 6, pp. 1548–1557, Jun. 2010.

[33] M. H. Pi, C. S. Tong, S. K. Choy, and H. Zhang, "A fast and effective model for wavelet subband histograms and its application in texture image retrieval," *IEEE Trans. Image Process.*, vol. 15, no. 10, pp. 3078–3088, Oct. 2006.
[34] L. Li, C. S. Tong, and S. K. Choy, "Texture classification using refined histogram," *IEEE Trans. Image Process.*, vol. 19, no. 5, pp. 1371–1378, May 2010.
[35] S. Arivazhagan, L. Ganesan, and T. G. Subash Kumar, "Texture classification using ridgelet transform," *Pattern Recognit. Lett.*, vol. 27, no. 16, pp. 1875–1883, 2006.
[36] D. D.-Y. Po and M. N. Do, "Directional multiscale modeling of images using the contourlet transform," *IEEE Trans. Image Process.*, vol. 15, no. 6, pp. 1610–1620, Jun. 2006.
[37] M. N. Do and M. Vetterli, "The contourlet transform: An efficient directional multiresolution image representation," *IEEE Trans. Image Process.*, vol. 14, no. 12, pp. 2091–2106, Dec. 2005.
[38] A. L. Da Cunha, J. Zhou, and M. N. Do, "The nonsubsampled contourlet transform: Theory, design, and applications," *IEEE Trans. Image Process.*, vol. 15, no. 10, pp. 3089–3101, Oct. 2006.
[39] G. Y. Che and B. Kegl, "Invariant pattern recognition using contourlets and AdaBoost," *Pattern Recognit.*, vol. 43, no. 3, pp. 579–583, Mar. 2010.
[40] Y. Dong and J. Ma, "Texture classification based on contourlet subband clustering," in *Proc. 7th Int. Conf. Intell. Comput.*, Zhengzhou, China, 2011, pp. 421–426.
[41] Y. Dong and J. Ma, "Bayesian texture classification based on contourlet transform and BYY harmony learning of Poisson mixtures," *IEEE Trans. Image Process.*, vol. 21, no. 3, pp. 909–918, Mar. 2012.
[42] Y. Dong and J. Ma, "Statistical contourlet subband characterization for texture image retrieval," in *Proc. 8th Int. Conf. Intell. Comput.*, Huangshan, China, 2012, pp. 500–507.
[43] G. Easley, D. Labate, and W.-Q. Lim, "Sparse directional image representations using the discrete shearlet transform," *Appl. Comput. Harmon. Anal.*, vol. 25, no. 1, pp. 25–46, Jul. 2008.
[44] K. Guo and D. Labate, "Optimally sparse multidimensional representation using shearlets," *SIAM J. Math. Anal.*, vol. 39, no. 1, pp. 298–318, 2007.
[45] K. Guo and D. Labate, "Characterization and analysis of edges using the continuous shearlet transform," *SIAM J. Imaging Sci.*, vol. 2, no. 3, pp. 959–986, Mar. 2009.
[46] S. Yi, D. Labate, G. R. Easley, and H. Krim, "A shearlet approach to edge analysis and detection," *IEEE Trans. Image Process.*, vol. 18, no. 5, pp. 929–941, May 2009.
[47] S. Weisberg, *Applied Linear Regression*. Hoboken, NJ, USA: Wiley, 2005.
[48] *The Brodatz Texture database* [Online]. Available: http://www.ux.uis.no/tranden/brodatz.html
[49] *The Vision Texture database* [Online]. Available: http://vismod.media.mit.edu/vismod/imagery/Vision Texture/vistex.html
[50] Y. Dong and J. Ma, "Wavelet-based image texture classification using local energy histograms," *IEEE Signal Process. Lett.*, vol. 18, no. 4, pp. 247–250, Apr. 2011.
[51] S. K. Choy and C. S. Tong, "Statistical wavelet subband characterization based on generalized gamma density and its application in texture retrieval," *IEEE Trans. Image Process.*, vol. 19, no. 2, pp. 281–289, Feb. 2010.

Yongsheng Dong received the Ph.D. degree in applied mathematics from Peking University, Beijing, China, in 2012.

He then joined the Information Engineering College, Henan University of Science and Technology, Luoyang, China. He is currently a Post-Doctoral Researcher with the Center for Optical Imagery Analysis and Learning, State Key Laboratory of Transient Optics and Photonics, Xi'an Institute of Optics and Precision Mechanics, Chinese Academy of Sciences, Xi'an, China. His current research interests include pattern recognition, machine learning, and computer vision.

Dacheng Tao (M'07-SM'12) is a Full Professor with the Center for Optical Imagery Analysis and Learning, State Key Laboratory of Transient Optics and Photonics, Xi'an Institute of Optics and Precision Mechanics, Chinese Academy of Sciences, Xi'an, China.

Xuelong Li (M'02–SM'07–F'12) is a Full Professor with the Center for Optical Imagery Analysis and Learning, State Key Laboratory of Transient Optics and Photonics, Xi'an Institute of Optics and Precision Mechanics, Chinese Academy of Sciences, Xi'an, China.

Jinwen Ma received the Ph.D. degree in probability theory and statistics from Nankai University, Tianjin, China, in 1992.

He is currently a Full Professor with the Department of Information Science at the School of Mathematical Sciences, Peking University, Beijing, China. During 1995 and 2003, he visited the Department of Computer Science and Engineering, The Chinese University of Hong Kong, several times as a Research Associate or a fellow. He was a Research Scientist at Amari Research Unit, RIKEN Brain Science Institute, Wakō, Japan, from 2005 to 2006. From 2011 to 2012, he visited the Department of Systems Medicine and Bioengineering, Houston Methodist Hospital Research Institute, Houston, TX, USA, as a Scientist. He has published over 100 academic papers on neural networks, pattern recognition, image processing, bioinformatics, and information theory.

Jiexin Pu is currently a Full Professor with the Information Engineering College, Henan University of Science and Technology, Luoyang, China. His current research interests include computer vision, pattern recognition, image processing, artificial intelligence, and cognitive science.